Influence of Carboxylic Acid Structure on the Kinetics of Polyurethane Foam Acidolysis to Recycled Polyol

Zach Westman, Baoyuan Liu, Kelsey Richardson, Madeleine Davis, Dingyuan Lim, Alan L. Stottlemyer, Christopher S. Letko, Nasim Hooshyar, Vojtech Vlcek, Phillip Christopher,* and Mahdi M. Abu-Omar*

Cite This: JACS Au 2024, 4, 3194−3204

Read Online

ACCESS | Metrics & More | Article Recommendations | Supporting Information

ABSTRACT: Closed-loop recycling of plastics is needed to bridge the gap between the material demands imposed by a growing global population and the depletion of nonrenewable petroleum feedstocks. Here, we examine chemical recycling of polyurethane foams (PUFs), the sixth most produced polymer in the world, through PUF acidolysis via dicarboxylic acids (DCAs) to release recyclable polyols. Acidolysis enables recycling of the polyol component of PUFs to high-quality materials, and while the influence of DCA structure on recycled PUF quality has been reported, there are no reports that examine the influence of DCA structure on the kinetics of polyol release. Here, we develop quantitative relationships between DCA structure and PUF acidolysis function for ~10 different DCA reagents. PUF acidolysis kinetics were quantified with ~1 s time resolution using the rate of carbon dioxide (CO_2) gas generation, which is shown to occur concomitantly with polyol release. Pseudo-zeroth-order rate constants were measured as a function of DCA composition, reaction temperature, and DCA concentration, and apparent activation barriers were extracted. Our findings demonstrate that DCA carboxyl group proximity and phase of transport are descriptors of PUF acidolysis rates, rather than expected descriptors like pK_a. DCAs with closer proximity acid groups exhibited faster PUF acidolysis rate constants. Furthermore, a shrinking core mechanism effectively describes the kinetic functional form of the kinetics of PUF acidolysis by DCAs. Measurements of acidolysis kinetics for model PUF (M-PUF) and end-of-life PUF (EOL PUF) confirm the applicability of our analysis to postconsumer materials. This work provides insights into the physical and chemical mechanisms controlling acidolysis, which can facilitate the development of efficient closed-loop PUF chemical recycling schemes.

KEYWORDS: polyurethane, acidolysis, kinetics, recycled polyol, carboxylic acid
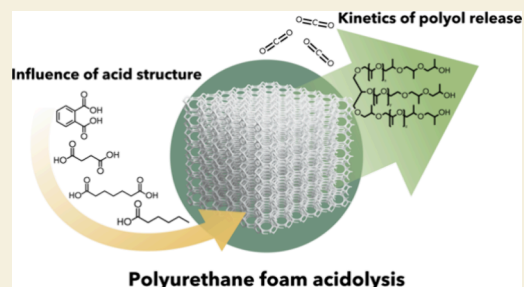
INTRODUCTION

Polyurethanes (PUs) are the sixth most produced polymer worldwide, with a global market size of 43 billion USD in 2021, corresponding to a global production of 18−24 million tons per year.[1−4] This number is expected to increase, with a predicted market size of 89 billion USD by 2030. PUs are a versatile class of materials with uses in a variety of consumer products, including mattresses, insulation, shoes, and the automotive industry, among others.[3] Rapid increase in demand for polymers has led to well-justified environmental concerns. Reliance on petroleum resources for the synthesis of polymers (plastics) contributes significantly to greenhouse gas emissions, and plastic waste is rapidly accumulating in our oceans and on land.[5,6] Unfortunately, the predominant approach to managing plastic waste is through incineration or landfill, which abandons much or all of the value of the material and pollutes the environment. For example, 1.3 million tons of PU waste is discarded annually in the USA.[7] Mechanical recycling of PU waste is typically performed by shredding or grinding the material and then either reusing the material as a filler or rebinding the material via extrusion, compression, or

molding.[8,9] These methods are simple, inexpensive, and eco-friendly and therefore have potential utility in the management of PU waste. However, they result in materials with inferior thermal and mechanical properties and can only be repeated a finite number of times and are therefore not a circular sustainable waste management practice.[3,10,11] In contrast, chemical recycling offers the possibility to convert plastic waste into valuable chemicals with little to no loss in quality, creating a pathway to a circular plastic economy.
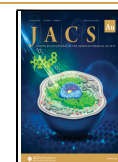
Chemical recycling of polyolefins has garnered significant interest in recent literature due to their large share of the global plastic market.[12−15] Both polyolefins and PUs rely on petroleum-based production methods, resulting in substantial generation of emissions and solid waste. However, synthesis of
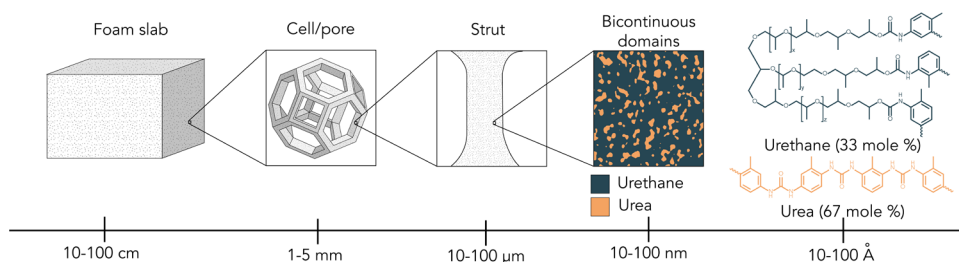
Scheme 1. Depiction of PU Foam Morphology at Various Length Scales[a]

[a]Individual cells appear spherical or polyhedral. Flexible PU foams contain soft segments (urethane bonds) and hard segments (urea bonds) that are distributed randomly throughout the structure in bicontinuous domains to give the foam the desired physical properties

polyether polyols (the major mass component for PUs) produces more than double the CO_2 emissions (2.9 kg CO_2/kg polyol) and solid waste (91 kg waste/10^3 kg polyol) than common polyolefins on a per-mass basis, including high-density polyethylene (1.8 kg CO_2/kg HDPE, 2.2 kg waste/10^3 kg HDPE), low-density polyethylene (1.9 kg CO_2/kg LDPE, 5.4 kg waste/10^3 kg LDPE), and polypropylene (1.6 kg CO_2/kg PP, 4.1 kg waste/10^3 kg PP).[16−18] Additionally, unlike polyolefins, PU materials contain reactive C−O and C−N bonds that allow for selective chemical decomposition without the need for high temperatures or expensive transition-metal catalysts. The recovery of polyols via PU chemical recycling therefore has viable chemical pathways under mild conditions, as well as clear economic and environmental incentives.

PU chemical depolymerization can be driven by chemolysis using reactants such as water (hydrolysis), glycols/alcohols (glycolysis/solvolysis), acids (acidolysis), and amines (aminolysis) to break chemical bonds within the PU structure into monomeric or oligomeric units. PU chemical recycling schemes generally focus on recovery of polyol, although some recent studies have attempted to recover isocyanates as well.[19] As of 2023, glycolysis and acidolysis have been commissioned on pilot or industrial scales, although neither have been widely commercialized.[11,13,20−23] Acidolysis uses organic acids, typically dicarboxylic acids (DCAs), to break down PU materials into carbon dioxide (CO_2), recycled polyol (repolyol), and amides. Acidolysis of PU is appealing compared to other chemical recycling approaches, as the reaction proceeds at relatively low temperatures (<200 °C) at atmospheric pressure with no added catalyst or solvent and produces repolyol that can be directly reused in the synthesis of new PU materials.[24] However, there is limited information in literature about how important parameters affect PU acidolysis rates. For example, there has been no systematic study of the influence of acid structure, acid loading, or temperature on the kinetics and product distribution of PU acidolysis.

PU acidolysis has been reported using maleic acid (MA), succinic acid (SA), phthalic acid (PA), and adipic acid (AA), although only a cursory comparison of SA and PA as acidolysis reagents has been made using bulk properties of the produced repolyol such as hydroxyl number (OH_{number}), acid value (AV), and molecular weight.[24−26] In addition, acidolysis has predominantly been studied with low (approximately stoichiometric) acid loadings, and at temperatures above 200 °C. Recent work from our group has shown that acidolysis with DCAs can proceed at temperatures as low as 140 °C, with either liquid- or vapor-phase DCAs in stoichiometric excess.[26,27] There exists no guiding chemical or physical

principles relating DCA structure to acidolysis rates, which are key for designing viable closed-loop chemical recycling schemes for postconsumer PU materials.

Here, we present a quantitative experimental analysis of PU acidolysis kinetics using 10 DCAs and two monocarboxylic acids with varying structure, pK_a, and melting point (T_m). The kinetics of polyol release during acidolysis of a model flexible, toluene diisocyanate (TDI)-based PU foam (M-PUF) was measured in the temperature range of 165−195 °C with ~1 s time resolution by quantifying volumetric CO_2 evolution. Correlations between acid concentration and acidolysis rate constants demonstrate that acidolysis performed below the T_m of the acid proceeds via vapor-phase transport from the solid acid to the M-PUF surface, whereas liquid-phase acid is the reactive phase above the T_m of the acid. Interestingly, acidolysis rate constants did not correlate with acid pK_a. Instead, the phase of the acid at reaction temperature and the intramolecular proximity of the DCA carboxyl groups to each other were found to be relevant descriptors of rate. DCAs with smaller distances between carboxyl groups exhibited faster acidolysis rates, suggesting potential cooperativity between the acid groups in the acidolysis mechanism. Based on trends in acidolysis apparent activation energies as a function of DCA structure and rate constants, we hypothesize that conformational preferences of DCAs (existing in ring or chain conformers) dictate the differences in acidolysis rates between acids. With the time resolution afforded by measurement of CO_2 evolution, we were able to observe the reaction order of acidolysis, which demonstrates that PUF acidolysis kinetics can be understood in the context of a shrinking core mechanism. To validate the applicability of these results on postconsumer PU products, kinetic measurements were also performed on end-of-life PU foam (EOL PUF). Our findings elucidate the transport and reaction mechanisms of PU acidolysis and offer the potential to begin developing acidolysis processes for scale-up.

RESULTS

Overview of M-PUF Acidolysis

The M-PUF used in this study was obtained from the Dow Chemical Company and was synthesized from TDI and VORANOL 8136 Polyol, a glycerine-initiated, nominal 3100 molecular weight heteropolymer triol that is typical of flexible foam formulations. SEM images show that individual cells are 1−5 mm in diameter and the struts range from 10 to 100 μm in width and length (Scheme 1). Due to TDI being added to the foam formulation in excess, most of the N bonds (~67% by moles) in the M-PUF are urea bonds formed by the

Scheme 2. Reaction of Urethane (Top) and Urea Moieties (Bottom) with Dicarboxylic Acids[a]
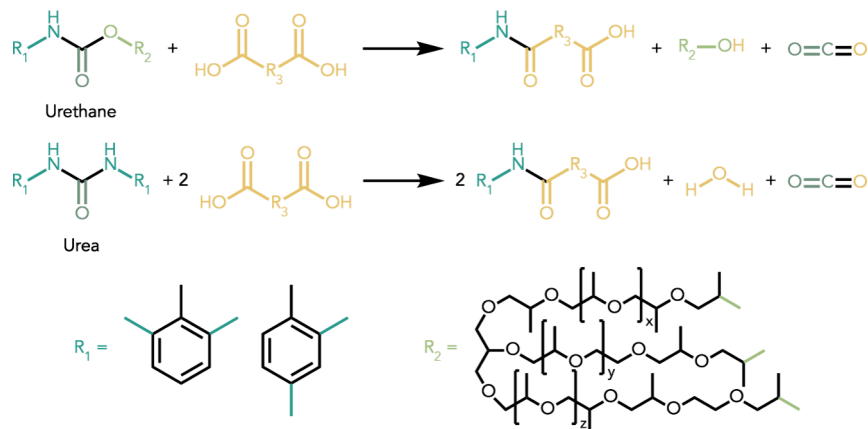
[a]Urethane bond acidolysis produces a polyol (R_2), a carboxylic amide, and CO_2, while urea bond acidolysis produces two carboxylic amides, CO_2, and H_2O. Reproduced from *ACS Macro Letters* 13 (4), 435−439. Copyright 2024 American Chemical Society.

reaction of TDI and water, despite polyol being the majority mass component. Previous characterization of similar flexible PUFs has shown that urea and urethane segments exist in bicontinuous morphologies with networks of interspersed domains between 5 and 10 nm in length.[28,29]

The reaction stoichiometry for PU acidolysis is summarized in Scheme 2. DCAs decompose both urethane and urea bonds. Decomposition of a urethane bond yields a repolyol, a carboxylic amide, and CO_2, while decomposition of a urea bond gives an amide, an amine, and CO_2. The amine and polyol product can further react with excess DCA to form an amide and polyol ester, respectively, and H_2O. Therefore, acid loadings below a molar ratio of 2:1 DCA:(urethane + urea bonds) may result in an incomplete reaction. In this report, we focus on the repolyol and CO_2 product formation, while future studies will address the product distribution and kinetics of N-containing product formation.

As mentioned above, we recently demonstrated that acidolysis with SA and PA can proceed at temperatures as low as 140 °C, even when the solid acid and the M-PUF are physically segregated.[27] The acid anhydrides of SA and PA (SAnh and PAnh, respectively) are volatile and unreactive for PU acidolysis but enable transport from the solid acids to M-PUF surfaces and subsequently hydrolyze with residual moisture in the M-PUF back to DCAs to drive acidolysis. Here, we examine 10 DCAs and 2 monoacids that exhibit a wide range of chemical and physical properties (summarized in Table 1), including carboxylic acids with sufficiently high melting points that are likely to perform acidolysis via vapor-phase transport of their respective anhydrides (e.g., PA and SA).[30−32]

Acidolysis of both urethane and urea bonds produces stoichiometric amounts of CO_2, and thus quantification of CO_2 generated during acidolysis offers an appealing, yet previously unreported approach for kinetic analysis of PU acidolysis. A general two-step reaction mechanism is proposed for PU acidolysis of urethane bonds, where the DCA facilitates repolyol release in the first step, followed by decarboxylation of a carbamic anhydride intermediate to create the amide product and CO_2 (Figure S1a). Density functional theory (DFT) calculations of the thermodynamics for these two steps were performed using model PU substrates; the entire polyol structure was not treated. The calculations suggest that polyol
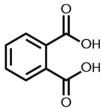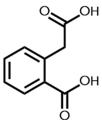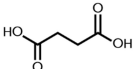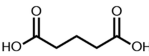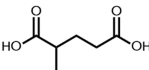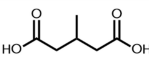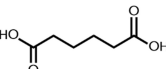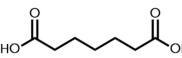
release is the thermodynamically unfavorable step in PU acidolysis and thus likely the rate-limiting step (Figure S1b). Therefore, CO_2 generation is hypothesized to be concomitant with repolyol release and thus can potentially be used to quantify acidolysis kinetics. This is experimentally justified below.

Kinetics of M-PUF Acidolysis with DCAs

Kinetic analysis of M-PUF acidolysis was executed in a temperature-controlled, closed-system reactor that allowed for volumetric quantification of CO_2 release with ∼1 s time resolution. A schematic of the apparatus and explanation of the measurements are provided in Figure S2 and in the SI, respectively. This approach for measuring PU acidolysis kinetics provides substantially improved time resolution as compared to the use of other 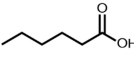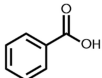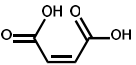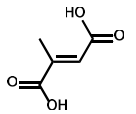analytical tools such as GPC or NMR and allows for kinetic measurements to be made *in situ*. Before reactions, the M-PUF was shredded into a powder with a particle diameter of 500−2000 μm based on scanning electron microscopy (SEM) analysis (Figure S3). The reaction temperature was kept below 200 °C in all acidolysis measurements to ensure that the M-PUF did not undergo significant thermal decomposition, which occurs on relevant time scales above 220 °C based on TGA measurements (Figure S4).[26] Isothermal TGA of the M-PUF was performed at 195 °C for 60 min. The sample showed <3% mass loss, confirming that thermal decomposition does not substantially occur at the reaction conditions evaluated here (Figure S5). Fourier transform infrared spectroscopy (FTIR) of the M-PUF before shredding, after shredding, and after heating at 195 °C for 1 h showed no significant changes, confirming that neither shredding nor heating caused degradation of the M-PUF (Figure S6).

To confirm that CO_2 evolution is concomitant with repolyol release, as hypothesized based on DFT calculations, the rate of repolyol formation was analyzed with gel permeation chromatography (GPC). Acidolysis of M-PUF with pimelic acid (PiA) at 195 °C was executed on time intervals between 20 and 180 min (see the SI for details), followed by sample collection and analysis by GPC and NMR. Figure 1a shows GPC distribution plots of the recovered repolyol from 20−60 min of reaction time. The disappearance of the high molecular weight shoulder with increasing reaction time confirms that repolyol release is complete in about 60 min. Figure 1b shows

Table 1. Substrate Scope for Kinetic Study of PUF Acidolysis with Associated Physical Properties

Name	Chemical Structure	Mol. Weight (g/mol)	T_m (°C) [30]	pKa$_1$ [31, 32]
Phthalic acid (PA)		166.1	207	2.95
Homophthalic acid (HPA)		180.2	183[1]	Unknown
Succinic acid (SA)		118.1	185	4.19
Glutaric acid (GA)		132.1	98	4.34
2-methylglutaric acid (2-MeGA)		146.1	77[1]	Unknown
3-methylglutaric acid (3-MeGA)		146.1	83[1]	Unknown
Adipic acid (AA)		146.1	152	4.42
Pimelic acid (PiA)		160.2	105	4.48
Hexanoic acid (HA)		116.2	-3	4.88
Benzoic acid (BA)		122.1	122	4.20
Maleic acid (MA)		116.1	135	1.92
Mesaconic acid (MCA)		130.1	208[1]	3.09

[1]The T_m of HPA, 2-MeGA, 3-MeGA, and MCA was measured by the authors.

the fractional amount of CO_2 evolved measured volumetrically *in situ* and the amount of repolyol released measured *ex-situ* by GPC as a function of reaction time. The fractional quantities were obtained through normalization by a reference chromatogram of VORANOL 8136 Polyol. The fractional repolyol and CO_2 release showed consistent time dependences, supporting the hypothesis that decarboxylation is fast compared to release of the polyol and confirming that the kinetics of repolyol formation via acidolysis could be monitored via quantification of CO_2 evolution (see Figure S7 and Table S2 for GPC peak fits). ^{1}H NMR of the products from the reactions in Figure 1 show that urea oligomer content is also qualitatively correlated with CO_2 evolution (Figure S8). The hypothesized carbamic

anhydride intermediate was not observed in ^{1}H or ^{13}C NMR (Figure S9 and Table S3), consistent with a mechanism in which decarboxylation is not rate-limiting during acidolysis of urethane or urea bonds (see the SI for details on product characterization). Figure 1 demonstrates the excellent time resolution of the volumetric CO_2 measurement in comparison to GPC or NMR, in addition to the experimental advantage of an *in situ* measurements rather than an approach where separate reactions are run to collect each data point in the time series. Furthermore, complete PUF decomposition was observed in <60 min at 195 °C, demonstrating that acidolysis was responsible for the observed chemistry rather than thermal degradation of the PUF (Figure S5).
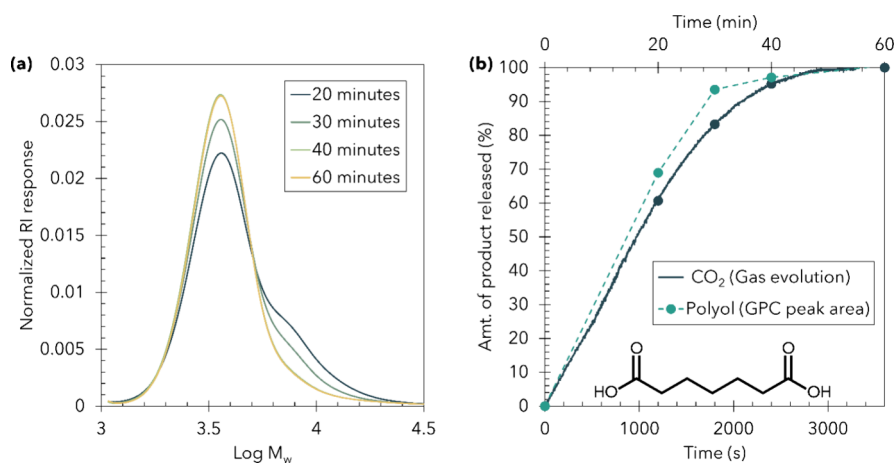
Figure 1. (a) Normalized refractive index (RI) response as a function of the molecular weight of the recovered polyol from acidolysis with PiA at 195 °C at various reaction times as measured by GPC. (b) Normalized percent of CO_2 (dark blue) and polyol (teal) released during acidolysis with PiA at 195 °C as a function of reaction time, measured by gas evolution and GPC, respectively. The fractional yields were calculated through normalization of the maximum amount of each product observed. The solid line is the experimental data associated with CO_2 release, and the dark blue data points are just shown for direct comparison to the GPC data. Reactions were executed with 0.5 g of M-PUF and 1.5 g of PiA under an inert (N_2) atmosphere.
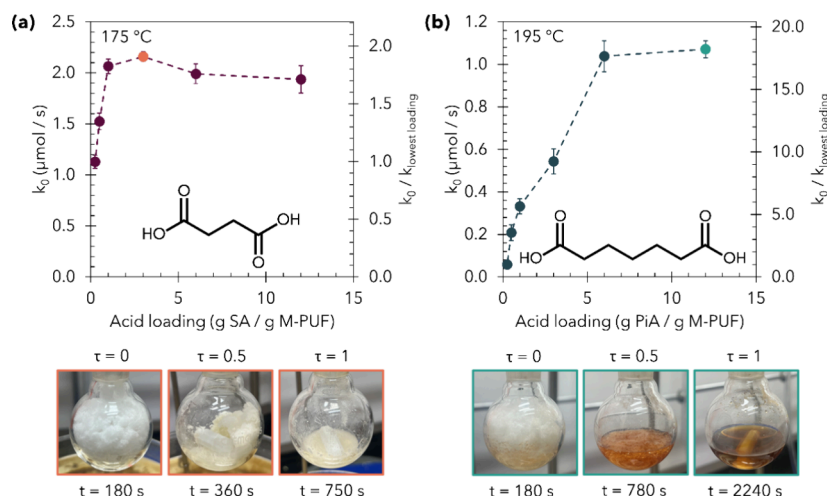

Figure 2. Pseudo-zeroth-order acidolysis rate constants, k_0, as a function of DCA loading for (a) SA and (b) PiA, along with photos of the reaction mixture at $\tau = 0$, 0.5, and 1 for the DCA loading at which the highest rate constant was measured (highlighted data point). τ was defined as the time at which gas evolution was complete. The dashed lines are to guide the eye.

The amount of CO_2 released from PU acidolysis was quantified via $Ca(OH)_2$ titration to produce $CaCO_3$, where stoichiometric CO_2 evolution with the decomposition of urethane and urea bonds was also observed (Figure S10). Furthermore, gas chromatography (GC-FID) of the gas phase after acidolysis detected only CO_2, confirming that CO_2 and H_2O were the only gaseous products formed (Figure S11). Thus, the volumetric CO_2 quantification provides high-fidelity kinetic data associated with PUF acidolysis and repolyol release, enabling quantitative kinetic analysis. We note that while the volume of gas generated during acidolysis stoichiometrically matched the expected volume of CO_2 from decomposition of both urethane and urea bonds for most reactions, the dehydration of certain DCAs (PA, HPA, and 3-MeGA) to their anhydrides at reaction temperatures resulted in excess gas (H_2O) generation (Figures S12 and S13). The SI contains a detailed description of the experiments.

Acid Concentration Dependence

Although several DCAs displayed nonlinear CO_2 evolution as a function of time at higher conversions of M-PUF, pseudo-zeroth-order fits of the initial 25% of CO_2 evolution were used to quantify the rate constants (see the SI, Figure S14 for details). The zeroth-order model generally fit all data sets well at low fractional conversion. The physical origin of zeroth-order kinetic trends is discussed further below.

Acidolysis of M-PUF was studied with varying concentrations of SA at 175 °C and PiA at 195 °C. These acids were chosen to highlight concentration-dependent PU acidolysis rates isolated for vapor-phase (SA) and liquid-phase (PiA) DCA transport. The mass ratio of DCA:M-PUF was varied from 0.25:1 to 12:1 for both acids. SA (T_m = 186 °C) was a solid at the explored reaction temperature (175 °C), meaning that transport of acid to the PUF surface likely occurred via volatile SAnh, followed by rehydration to form SA at the PUF surface. A predominantly solid reaction mixture was observed for the entirety of the reaction, although the formation of
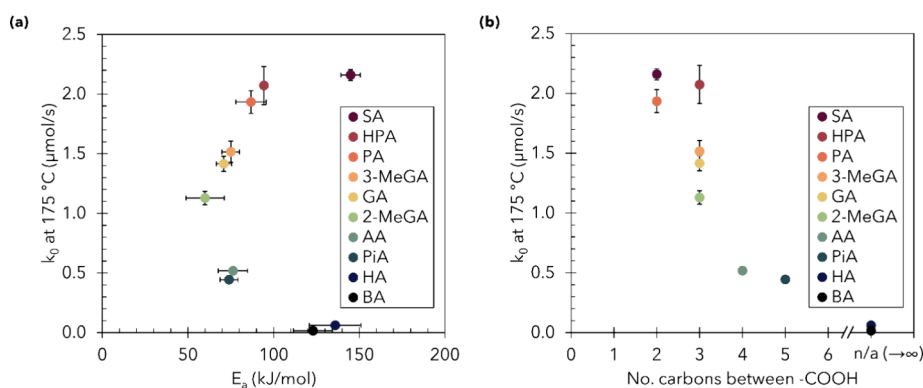
Figure 3. (a) Pseudo-zeroth-order rate constants, k_0, measured at 175 °C plotted as a function of apparent activation energy, E_a, for acidolysis with various DCAs. (b) k_0 for acidolysis at 175 °C plotted as a function of the distance between −COOH groups for various DCAs and two monoacids (HA and BA, which are assumed to have effectively infinite distance between COOH groups). All reactions were run with 0.5 g of M-PUF under an inert (N_2) atmosphere at DCA:PU mass ratios that maximized the observed rate constants.

liquid repolyol resulted in a viscous melt as the reaction proceeded (Figure 2a). The observed pseudo-zeroth-order rate constants (k_0) for M-PUF acidolysis by SA exhibited minimal concentration dependence, varying by a factor of ~2 with a ~50-fold variation in acid mass added to the reactor. This is consistent with vapor-phase transport of the reactive species— the concentration of acid (or acid anhydride) vapor in the reactor is limited by its saturation vapor pressure at a given temperature and will therefore not change with increasing mass of solid acid. The maximum observed acidolysis rate constant was at a DCA:PUF loading of 3:1. The slight decrease in rate constant observed at low acid loadings is likely due to the decreased acid surface area, which may increase the time required to achieve saturation vapor pressure of the volatile SAnh. At higher acid loadings, the rate also decreases, likely due to the increased mass in the reactor imposing limitations to the rate of heating of the reactant mixture, although these changes are small and within measurement uncertainty.

In contrast, PiA rapidly melted as the reactor heated to 195 °C, and as the reaction proceeded, a homogeneous liquid reaction mixture formed (Figure 2b). The measured rate constant of acidolysis by PiA at 6:1 DCA:PU was ~18 times higher than the rate constant at 0.25:1 DCA:PU, showing a stark contrast to SA. Interestingly, the rate plateaued above a loading of 6:1 mass ratio of DCA:PU. Similar saturation values of rate constants as a function of DCA:PU ratio were observed for all acids operated as liquids above their respective T_m (3-MeGA, GA, 2-MeGA, AA, and PiA), although the concentration required for saturation was dependent on the acid and the reaction temperature (Figure S15). Because acidolysis is an irreversible reaction and the reaction was run without a solvent, the increase in rate constant and subsequent plateau with increasing liquid DCA amount added to the reaction was attributed to increased foam wetting (i.e., saturation of the foam surface with liquid acid), meaning that the measured rate constant below the plateau is a combined result of both chemical reaction kinetics and mass transport kinetics. Above the plateau, the surface of the foam becomes saturated and mass transfer effects cease to be rate-limiting. The differences in DCA loading required to reach saturation rates as a function of DCA and temperature are likely derived from a combination of the DCA melting rate and subsequent rate of M-PUF acidolysis. The wide variation in observed rate constant with acid loading for 3-MeGA, GA, 2-MeGA, AA, and PiA suggests

that these acids predominantly exist in the liquid phase as reaction with M-PUF proceeds, consistent with their T_m.

Temperature and Acid Dependence

The influence of temperature on acidolysis kinetics was studied in the range of 165−195 °C. As discussed above, there were substantial variations in acidolysis rate constants as a function of acid concentration for acids that were liquid at reaction temperatures. Based on the assumption that the maximum rate constants observed occurred when saturation coverage of the foam by DCA was attained, temperature-dependent experiments were run at acid loadings where the highest rate constants were observed. The influence of acid concentration on acidolysis rates was not studied for PA and HPA due to the formation of anhydride. Thus, a 3:1 DCA:M-PUF (by mass) loading was chosen, as this loading was ideal for SA acidolysis, which is similarly hypothesized to react with PUF via vapor-phase anhydride transport. When comparing the kinetics of PUF acidolysis for the scope of DCAs shown in Table 1, the measured rate constants and apparent activation energies varied significantly across the tested acids (Figure 3 and Table S4).

DCAs that were liquid phase at reaction temperatures (GA, AA, PiA, 2-MeGA, 3-MeGA) exhibited consistent acidolysis apparent activation energies (E_a) of approximately 75 kJ/mol, although the pseudo-zeroth-order rate constants varied by ~4-fold. This E_a is reasonable for an exothermic reaction in the tested temperature range and is hypothesized to represent the inherent activation energy for PUF acidolysis, as mass transport limitations would result in a lower E_a. Acids that were solid at reaction temperatures (and transported through the vapor phase via anhydrides to the PUF surface) exhibited higher acidolysis E_a. SA exhibited the highest E_a (145 kJ/mol), despite having the highest rate constant of all acids tested (Figure 3a). Interestingly, the enthalpy of sublimation of SA is approximately 115 kJ/mol.[33] We hypothesize that the rate of M-PUF acidolysis by SA is limited by the rate of SAnh vaporization and transport to the M-PUF surface, thus leading to an E_a that is influenced by the heat of sublimation. Similarly, PA and HPA exhibited higher E_a than acids that existed as liquids at reaction temperature even after correcting for anhydride formation (Figures S16 and S17), indicating vapor-phase transport of these acids (likely via their anhydrides) to the M-PUF surface. Thus, we hypothesize that the PU acidolysis rate constants reported for DCAs that

transport via the vapor phase likely underestimate the inherent acidolysis rate constants.

For the scope of DCAs considered here, including those reacting through different transport mechanisms, the PU acidolysis rate constants varied by fivefold at 175 °C. The difference in rate constants between GA, 3-MeGA, AA, and PiA, which all had the same E_a, is particularly interesting, suggesting that the difference in their observed kinetics is predominantly due to differences in the pre-exponential factor. The observed rate constants did not correlate with DCA pK_a, melting temperature, or vapor pressure. The only physical parameter considered that correlated well with observed rate constants was the number of carbons between carboxyl groups on the DCAs (Figure 3b). As the carbon chain length between −COOH groups increased, the rate decreased, despite the reaction stoichiometry requiring only one −COOH group to decompose a urethane or urea bond.

To further test the influence of a second −COOH group on M-PUF acidolysis, kinetics were measured for two mono-carboxylic acids, hexanoic acid (HA) and benzoic acid (BA). Both HA and BA displayed substantially (ca. 5−100×) slower rate constants than any DCA tested. This suggests that the interaction of both carboxyl groups in DCAs with urethane and urea bonds may enable faster rates of acidolysis.

To substantiate this hypothesis, M-PUF acidolysis was tested with MA and mesaconic acid (MCA), which both have the same number of backbone carbons as SA but contain a double bond that either forces (MA) or prevents (MCA) proximity of two carboxyl groups (Table S5). For example, MCA is inhibited from internally rearranging such that the carboxyl end groups can directly interact (i.e., form intra-molecular hydrogen bonds). Figure 4 shows the gas evolution
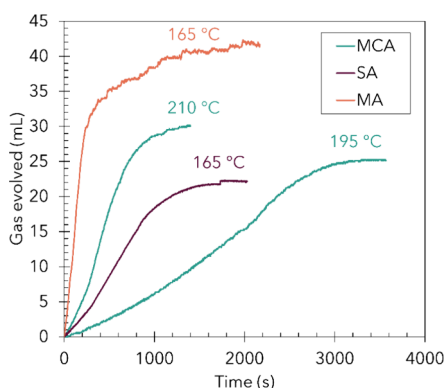

Figure 4. Gas evolution as a function of time from M-PUF acidolysis with MA and SA at 165 °C and MCA at 195 and 210 °C. All experiments were run with 0.5 g of M-PUF under an inert (N_2) atmosphere. It is noted that higher than expected gas evolution associated with CO_2 production from acidolysis observed for MA (and MCA at higher temperature) is due to water vapor formation via DCA anhydride formation.

plots for M-PUF acidolysis by these acids, as well as SA. While water formation from MA dehydration to maleic anhydride (MAnh) complicates kinetic analysis, gas evolution from acidolysis with MA completes faster than SA. This is consistent with the hypothesis that having DCA carboxyl groups in proximity promotes PUF acidolysis rates. Interestingly, MCA showed a much slower rate of acidolysis than SA and MA, despite having the same number of carbons between its carboxyl groups. A reaction with MCA at 210 °C (above its

T_m) still proceeded slower than MA at 165 °C, precluding the possibility of slow vapor-phase transport as a cause of the observed rate of MCA acidolysis. Apparent pseudo-zeroth-order rate constants, k_0, were 4.9 μmol/s (MA at 165 °C), 1.1 μmol/s (MCA at 210 °C), 0.8 μmol/s (SA at 165 °C), and 0.2 μmol/s (MCA at 195 °C). Thus, the general trend observed in Figure 3b, along with the differences in PU acidolysis reactivity of MA and MCA, support the hypothesis that it is not solely the proximity, but also the interaction between DCA carboxyl groups that facilitates faster rates of M-PUF acidolysis.

As mentioned above, the apparent reaction order varied with both temperature and DCA composition. Figure 5 shows CO_2 evolution during PUF acidolysis by SA and PiA, the tested DCAs with the fastest and slowest observed rates, at their respective saturation mass loadings as representative examples. DCAs with faster relative PU acidolysis kinetics, such as SA, displayed pseudo-zeroth-order behavior, while slower acids (such as PiA) exhibited rate dependence on the M-PUF concentration. However, within the first ~25% of gas evolution, the data was reasonably fit by the zeroth-order model. A pseudo-first-order model provided a poor fit for all acids, suggesting an apparent reaction order in PU of between zero and one (Figure S18). Additionally, it is interesting to note that gas evolution only showed one kinetic regime, despite the foam containing a mix of urethane and urea bonds, which are expected to have distinct kinetics. SEM images of partially decomposed M-PUF show that DCA likely eats away at the exterior of the foam surface, causing the polymer particles to decrease in volume as the reaction proceeds (Figures S3 and S19). These observations will be discussed more in the discussion section below.

Validation with EOL PUF

To assess the influence of PUF composition and contamination on the measured acidolysis rates, experiments were repeated on a mixture of postconsumer, end-of-life (EOL) mattress foam waste from Europe (Figure 6a). The obtained material was not cleaned or sorted prior to use, suggesting that the foam contains a variety of PUF compositions (likely synthesized with different precursors and in different compositions) and contaminants. EOL PUF acidolysis was tested with SA and PA at 175 °C and GA from 165 to 195 °C (Figure 6b). Pseudo-zeroth-order rate constants, E_as, and reaction orders with EOL PUF were similar to those found for M-PUF. In fact, EOL PUF acidolysis displayed slightly faster kinetics than M-PUF acidolysis (Figure 6c). While the exact composition of the EOL PUF is unknown, the results suggest that kinetics observed for M-PUF acidolysis reported here via CO_2 evolution measurements are applicable to a wide range of PUF materials and do not appear to be particularly sensitive to small variations in composition and PUF particle size.

■ DISCUSSION AND CONCLUSIONS

The direct measurement of PUF acidolysis kinetics with excellent time resolution for a wide scope of DCAs resulted in a number of interesting observations that warrant further discussion. First, a comparison of the time-dependent CO_2 evolution and polyol release demonstrated that CO_2 evolution can be used as an *in situ* measurement of PUF acidolysis kinetics. Second, it was broadly observed that DCAs reacted with PUF surfaces from the liquid phase when reactions were run above the T_m of the DCA but that vapor-phase transport of DCAs (likely via volatile acid anhydrides that rehydrate at the
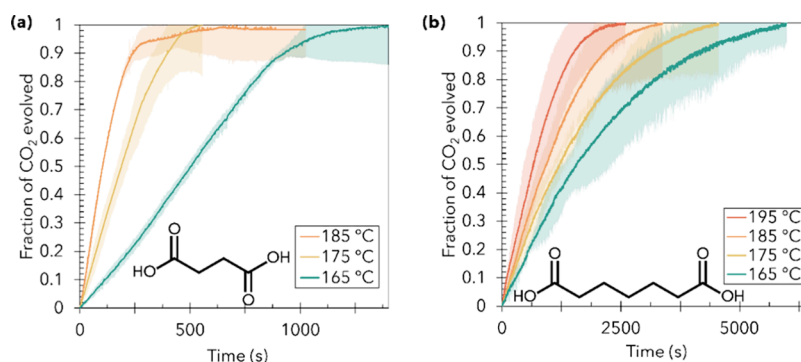
Figure 5. Fractional CO_2 evolution as a function of time during acidolysis of M-PUF with (a) SA from 165 to 185 °C and (b) PiA from 165 to 195 °C. Shaded regions represent 95% confidence intervals based on three repeated trials at each temperature. All reactions were run with 0.5 g of M-PUF under an inert (N_2) atmosphere.
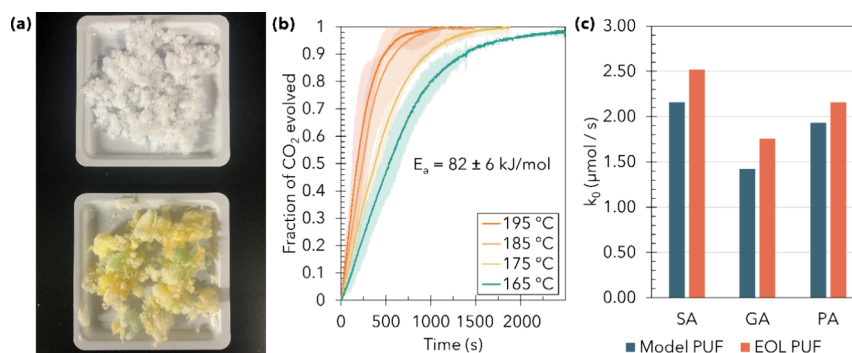

Figure 6. (a) Photos of shredded M-PUF (top) and EOL PUF (bottom). (b) Fractional CO_2 evolution during acidolysis of EOL PUF with GA from 165 to 195 °C. (c) Comparison of pseudo-zeroth-order rate constants, k_0, for acidolysis with M-PUF and EOL PUF at 175 °C with SA, GA, and PA. All experiments were run with 0.5 g M-PUF under an inert (N_2) atmosphere. EOL PUF acidolysis kinetic experiments were performed without additional shredding.

foam surface) enabled M-PUF acidolysis when operating below the T_m of the DCA. Apparent activation energies were consistent for DCAs reacting from the liquid phase, while higher barriers were observed for DCAs reacting via vapor-phase transport, suggesting that the measured rates of acidolysis were limited by the rate of vapor-phase transport when the DCAs were reacted below their T_m. This suggests that the observed acidolysis rate constants for DCAs that transported via the vapor phase are likely underestimates of inherent acidolysis kinetics. Despite inherent kinetic differences in acidolysis based on the DCA phase, a trend was observed between acidolysis rate constants and the DCA carboxyl group proximity. This is interesting from a fundamental perspective as the trend points to a cooperative role of both carboxyl acid groups in the rate-limiting step, and also from a process design perspective, as a vapor-phase reaction has the potential to reduce the required amount of acidolysis reagent and complexity of product separations.

The constancy of apparent activation energies for the DCAs that reacted from the liquid phase suggests the observed differences in rate between these acids are solely due difference in the pre-exponential factors. Taking the trends in apparent rate constant, apparent pre-exponential factor, and apparent activation energy with carboxyl group proximity into account, we hypothesize that the ability (or inability) of the DCA backbone to rearrange and allow the participation of both of its carboxyl groups in the transition state for the rate-limiting step is responsible for the differences in rate between DCAs. While the mechanistic role of a second carboxyl group in the reaction

is unclear given the reaction stoichiometry, it seems likely that acid hydrogen-bonding interactions influence the rate of the acidolysis reaction. One possible explanation for the observed trend between carboxyl proximity and rate is that intramolecular hydrogen bonding between two hydroxyl groups on the DCA (resulting in a ring-like acid conformer) stabilizes the transition state and facilitates reactivity. DCAs are known to exist in a distribution of conformations.[34,35] Acids with more proximal carboxyl groups may be more likely to form the ring conformer, resulting in a higher concentration of active species in the reaction mixture, while acids with more distant carboxyl groups may be more likely to exist in chain conformers. This hypothesis would be consistent with the fast rate of acidolysis with MA, which is forced by its double bond into a ring conformation, and the slow rate of acidolysis with MCA, which cannot form a ring conformer due to its *trans* configuration. It is noteworthy that the monocarboxylic acids, which also cannot form intramolecular hydrogen bonds, have a higher apparent activation energy despite transporting as liquids. This, again, is consistent with the importance of hydrogen-bonding interactions rather than electronics in dictating acidolysis rates, given that BA and HA have similar pK_a to DCAs that transport as liquids (Table 1). However, other possibilities, such as hydrogen bonding between one carboxyl of a DCA and the PUF surface providing an "anchor" to facilitate access of the other carboxyl to an active bond, cannot be ruled out based on these results alone.

Another surprising observation is the difference in the apparent reaction order in M-PUF concentration as a function

of DCA structure. See for example Figure 5, where both apparent zeroth-order and higher-order dependences of rate on M-PUF concentration are observed. Particularly for acids that perform PU acidolysis from the liquid phase, pseudo-first-order kinetics in M-PUF concentration might be expected, as DCA is in large molar excess to M-PUF in the reaction mixture. However, none of the CO_2 evolution traces fit well to a first-order model (Figure S18), even with acids that react from the liquid phase at saturation loadings where mass transfer is expected to be fast compared to reaction kinetics. On the other hand, it also seems unlikely that M-PUF acidolysis could exhibit a zeroth-order dependence on M-PUF concentration, given that it is the limiting reagent.

Shrinking core models have previously been used to describe the kinetics of PET depolymerization,[36−38] biomass gasification/liquefaction,[39−41] and ore leaching processes,[42,43] among others. The central feature of a shrinking core model is that a solid reactant is changing in volume (and surface area) as it is consumed (or generated) during the reaction and further that mass transport to or from the solid surface may control the observed rate. We hypothesize that M-PUF acidolysis kinetics may fit well to a shrinking core model. The apparent zeroth-order kinetics observed for M-PUF acidolysis with SA and PA are consistent with a so-called film-diffusion-controlled reaction, in which the kinetics of acidolysis are sufficiently fast that the concentration of DCA vapor (or DCA anhydride vapor) at the foam surface approaches zero, and the rate becomes dictated solely by the unchanging bulk concentration of the vapor-phase reactant (i.e., by diffusion of acid vapor through the film layer). We hypothesize that as the inherent acidolysis reaction rate slows (as the distance between proximal carboxyls on the DCA increases) and the concentration of acid at the M-PUF surface becomes non-negligible (as would be the case in the liquid acid phase), the observed rate of reaction becomes controlled by the rate of acidolysis rather than acid transport. This is consistent with the nonlinear (and non-first-order) kinetics observed for DCAs with slower rates of acidolysis. A shrinking core model may also be able to justify the single kinetic regime observed during CO_2 evolution, which was unexpected given the two types of bonds (urethane and urea) reacting during acidolysis. This could be due to either the role of diffusion of DCAs to the PUF surface being rate controlling or the bicontinuous nature of M-PUF structures that may require decomposition of urea bonds to expose urethane bonds or vice versa. Future efforts will focus on detailed modeling of the high fidelity acidolysis kinetics to extract rigorous kinetic parameters, rather than the apparent parameters presented here.

The findings of this study offer a framework to assist in designing large-scale closed-loop PU recycling processes. The results presented expand the scope of reaction conditions investigated and demonstrate how the acid structure affects both the mechanism of acid transport and the inherent kinetics of the acidolysis reaction. Furthermore, the comparable kinetics observed for acidolysis of EOL PUF indicate that the rate of acidolysis is agnostic to small variations in foam composition. The insights reported here provide a starting point for the design of innovative and scalable closed-loop acidolysis processes. However, more work must be done to fully realize PU chemical recycling on an industrial scale. Future studies of PU acidolysis should focus on the effects of heat and mass transfer on the rate of acidolysis, particularly at larger scales and with acids that transport as vapors.

Additionally, understanding of the product distribution, kinetics, and separations of N-containing byproducts from acidolysis is still limited and should be explored in detail. Ultimately, we hope that this study provides a stepping stone toward the chemical recycling of PU materials and progresses toward a circular plastic economy.

■ ASSOCIATED CONTENT

Ⓢ Supporting Information

The Supporting Information is available free of charge at https://pubs.acs.org/doi/10.1021/jacsau.4c00495.

Materials and methods, grinding pretreatment, characterization of M-PUF, DFT calculations, PUF acidolysis kinetic measurement setup, characterization of M-PUF, characterization of products, time-dependent GPC characterization of repolyol from M-PUF acidolysis with PiA, time-dependent ^1H and quantitative ^{13}C NMR spectroscopy of products from M-PUF acidolysis with PiA, analysis of gas-phase products from acidolysis, anhydride control experiments, PUF acidolysis $CaCO_3$ collection setup, GC-FID of gaseous products, fitting of gas evolution data, modified fitting procedure for PA, HPA, and 3-MeGA, SEM of M-PUF before and after reaction, parameters from Gaussian peak deconvolution of monomer peaks from GPC experiments, ^1H and quantitative ^{13}C NMR peak assignments, tabulated kinetic parameters for M-PUF acidolysis, and structures and physical properties of DCAs used for comparison studies to examine importance of acid carboxyl group interactions (PDF)

■ AUTHOR INFORMATION

Corresponding Authors

Phillip Christopher − *Department of Chemical Engineering, University of California, Santa Barbara, Santa Barbara, California 93106-5080, United States;* ⓞ orcid.org/0000-0002-4898-5510; Email: pchristopher@ucsb.edu

Mahdi M. Abu-Omar − *Department of Chemical Engineering, University of California, Santa Barbara, Santa Barbara, California 93106-5080, United States; Department of Chemistry and Biochemistry, University of California, Santa Barbara, Santa Barbara, California 93106-9510, United States;* Email: mabuomar@ucsb.edu

Authors

Zach Westman − *Department of Chemical Engineering, University of California, Santa Barbara, Santa Barbara, California 93106-5080, United States*

Baoyuan Liu − *Department of Chemistry and Biochemistry, University of California, Santa Barbara, Santa Barbara, California 93106-9510, United States*

Kelsey Richardson − *Department of Chemical Engineering, University of California, Santa Barbara, Santa Barbara, California 93106-5080, United States*

Madeleine Davis − *Department of Chemistry and Biochemistry, University of California, Santa Barbara, Santa Barbara, California 93106-9510, United States*

Dingyuan Lim − *Department of Chemistry and Biochemistry, University of California, Santa Barbara, Santa Barbara, California 93106-9510, United States*

Alan L. Stottlemyer − *The Dow Chemical Company, Midland, Michigan 48642, United States*

Christopher S. Letko − *The Dow Chemical Company, Midland, Michigan 48642, United States*

Nasim Hooshyar − *The Dow Chemical Company, 4542 NH Hoek, The Netherlands*

Vojtech Vlcek − *Department of Chemistry and Biochemistry, University of California, Santa Barbara, Santa Barbara, California 93106-9510, United States; Department of Materials, University of California Santa Barbara, Santa Barbara, California 93016-5050, United States*

Complete contact information is available at:
https://pubs.acs.org/10.1021/jacsau.4c00495

Notes

The authors declare no competing financial interest.

■ REFERENCES

(1) *Global Polyurethane Market worth US$ 88.76 billion by 2030 with a CAGR of 2.50%*; 2021.

(2) *Polyurethane Foam Market by Type (Rigid Foam, Flexible Foam, Spray Foam), End-use Industry (Building & Consutrction, Bedding & Furniture, Automotive, Electronics, Footwear, Packaging) and Region - Global Forecast to 2026*; 2021.

(3) Kemona, A.; Piotrowska, M. Polyurethane recycling and disposal: Methods and prospects. *Polymers* **2020**, *12* (8), 1752.

(4) Nerland, I. L. et al. *Microplastics in marine environments: Occurrence, distribution and effects*; Niva: 2014.

(5) Lau, W. W. Y.; et al. Evaluating scenarios toward zero plastic pollution. *Science* **2020**, *369* (6510), 1455−1461.

(6) Borrelle, S. B.; et al. Predicted growth in plastic waste exceeds efforts to mitigate plastic pollution. *Science* **2020**, *369* (6510), 1515−1518.

(7) Nikje, M. M. A.; Garmarudi, A. B.; Idris, A. B. Polyurethane waste reduction and recycling: From bench to pilot scales. *Des. Monomers Polym.* **2011**, *14* (5), 395−421.

(8) Rossignolo, G.; Malucelli, G.; Lorenzetti, A. Recycling of Polyurethanes: where we are and where we are going. *Green Chem.* **2024**, 1132.

(9) Banik, J.; et al. Review on disposal, recycling and management of waste polyurethane foams: a way ahead. *Waste Management & Research* **2023**, *41* (6), 1063−1080.

(10) Schyns, Z. O. G.; Shaver, M. P. Mechanical recycling of packaging plastics: A review. *Macromol. Rapid Commun.* **2021**, *42* (3), No. 2000415.

(11) Zia, K. M.; Bhatti, H. N.; Bhatti, I. A. Methods for polyurethane and polyurethane composites, recycling and recovery: A review. *React. Funct. Polym.* **2007**, *67* (8), 675−692.

(12) Liu, B.; et al. Opportunities in Closed-Loop Molecular Recycling of End-of-Life Polyurethane. *ACS Sustainable Chem. Eng.* **2023**, *11* (16), 6114−6128.

(13) Simón, D.; et al. Recycling of polyurethanes from laboratory to industry, a journey towards the sustainability. *Waste Management* **2018**, *76*, 147−171.

(14) Behrendt, G.; Naber, B. W. The chemical recycling of polyurethanes. *J. Univ. Chem. Technol. Metall.* **2009**, *44* (1), 3−23.

(15) Goring, P. D.; Priestley, R. D. Polymer recycling and upcycling: recent developments toward a circular economy. *JACS Au* **2023**, *3* (10), 2609−2611.

(16) PlasticsEurope *Eco-profiles and Environmental Product Declarations of the European Plastics Manufacturers: Polypropylene (PP)*; 2016.

(17) PlasticsEurope *Eco-profiles and Environmental Product Declarations of the European Plastics Manufacturers: High-density Polyethylene (HDPE), Low-density Polyethylene (LDPE), Linear Low-density Polyethylene (LLDPE)*; 2016.

(18) PlasticsEurope *Eco-profile of long and short chain polyether polyols for polyurethane products*; ISOPA: 2021.

(19) O'Dea, R. M.; et al. Toward Circular Recycling of Polyurethanes: Depolymerization and Recovery of Isocyanates. *JACS Au* **2024**, *4* (4), 1471−1479.

(20) Heiran, R.; Ghaderian, A.; Reghunadhan, A.; Sedaghati, F.; Thomas, S.; Haghighi, A. H. Glycolysis: An efficient route for recycling of end of life polyurethane foams. *J. Polym. Res.* **2021**, *28*, 22.

(21) *Innovative approach to conversion of flexible PU foam residues into polyol on an industrial scale*; H & S Anlagentechnik GmbH.

(22) SolTysiński, M.; et al. Conversion of polyurethane technological foam waste and post-consumer polyurethane mattresses into polyols−industrial applications. *Polimery* **2018**, *63* (3), 234−238.

(23) Kanchanapiya, P.; Intaranon, N.; Tantisattayakul, T. Assessment of the economic recycling potential of a glycolysis treatment of rigid polyurethane foam waste: A case study from Thailand. *Journal of Environmental Management* **2021**, *280*, No. 111638.

(24) Grdadolnik, M.; et al. Insight into chemical recycling of flexible polyurethane foams by acidolysis. *ACS sustainable chemistry & engineering* **2022**, *10* (3), 1323−1332.

(25) Godinho, B.; et al. Recycling of polyurethane wastes using different carboxylic acids via acidolysis to produce wood adhesives. *J. Polym. Sci.* **2021**, *59* (8), 697−705.

(26) Liu, B.; et al. Polyurethane Foam Chemical Recycling: Fast Acidolysis with Maleic Acid and Full Recovery of Polyol. *ACS Sustainable Chem. Eng.* **2024**, *12* (11), 4435−4443.

(27) Liu, B.; et al. Vapor-Phase Dicarboxylic Acids and Anhydrides Drive Depolymerization of Polyurethanes. *ACS Macro Lett.* **2024**, *13*, 435−439.

(28) Aou, K.; et al. Two-domain morphology in viscoelastic polyurethane foams. *Polymer* **2015**, *56*, 37−45.

(29) Aou, K.; et al. Characterization of polyurethane hard segment length distribution using soft hydrolysis/MALDI and Monte Carlo simulation. *Polymer* **2013**, *54* (18), 5005−5015.

(30) Acree, J. W. E.; Chickos, J. S. Phase Change Data. In *NIST Chemistry WebBook*, NIST Standard Reference Database Number 69; National Institute of Standards and Technology: 2024.

(31) Williams, R. *Organic Chemistry Data*. Bordwell pKa Table; 2024 https://organicchemistrydata.org/hansreich/resources/pka/.

(32) Wang, B. Y.; et al. Selective Separation of Acetic and Hexanoic Acids across Polymer Inclusion Membrane with Ionic Liquids as Carrier. *Int. J. Mol. Sci.* **2019**, *20* (16), 3915.

(33) Bilde, M.; et al. Saturation vapor pressures and transition enthalpies of low-volatility organic molecules of atmospheric relevance: from dicarboxylic acids to complex mixtures. *Chem. Rev.* **2015**, *115* (10), 4115−4156.

(34) Nguyen, T. H.; Hibbs, D. E.; Howard, S. T. Conformations, energies, and intramolecular hydrogen bonds in dicarboxylic acids: implications for the design of synthetic dicarboxylic acid receptors. *Journal of computational chemistry* **2005**, *26* (12), 1233−1241.

(35) Moskovits, M.; Suh, J. Conformation of mono-and dicarboxylic acids adsorbed on silver surfaces. *J. Am. Chem. Soc.* **1985**, *107* (24), 6826−6829.

(36) Yoshioka, T.; Motoki, T.; Okuwaki, A. Kinetics of hydrolysis of poly (ethylene terephthalate) powder in sulfuric acid by a modified shrinking-core model. *Industrial & engineering chemistry research* **2001**, *40* (1), 75−79.

(37) López-Fonseca, R.; González-Velasco, J.; Gutiérrez-Ortiz, J. A shrinking core model for the alkaline hydrolysis of PET assisted by

tributylhexadecylphosphonium bromide. *Chemical Engineering Journal* **2009**, *146* (2), 287−294.

(38) Yoshioka, T.; Okayama, N.; Okuwaki, A. Kinetics of hydrolysis of PET powder in nitric acid by a modified shrinking-core model. *Industrial & engineering chemistry research* **1998**, *37* (2), 336−340.

(39) Jayathilake, M.; Rudra, S.; Rosendahl, L. A. Hydrothermal liquefaction of wood using a modified multistage shrinking-core model. *Fuel* **2020**, *280*, No. 118616.

(40) Seo, D. K.; et al. Gasification reactivity of biomass chars with CO2. *Biomass and Bioenergy* **2010**, *34* (12), 1946−1953.

(41) Babu, B.; Chaurasia, A. Heat transfer and kinetics in the pyrolysis of shrinking biomass particle. *Chem. Eng. Sci.* **2004**, *59* (10), 1999−2012.

(42) Veglio, F.; et al. Shrinking core model with variable activation energy: a kinetic model of manganiferous ore leaching with sulphuric acid and lactose. *Hydrometallurgy* **2001**, *60* (2), 167−179.

(43) Safari, V.; et al. A shrinking particle—shrinking core model for leaching of a zinc ore containing silica. *Int. J. Miner. Process.* **2009**, *93* (1), 79−83.